

Structural Analysis of the B-24 Liberator Fuselage Final Report

— Prepared for —

Dr. Craig G. Merrett

Associate Professor, Mechanical & Aerospace Engineering
Clarkson University

Heather Thies

Director of Education & Director of Volunteers,
National Museum of the Mighty Eighth Air Force
Pooler, GA, USA

— Prepared by —

Jonah Bajema (0941896)
Tyler Brooks (0759179)
Dante Cusolito (0944905)
Benjamin Ellis (0942309)

G01-FRCS-01

Undergraduate Students, Mechanical & Aerospace Engineering
AE 458: Design of Aircraft Structures
Clarkson University

April 2023

Abstract

The Consolidated B-24 is a multi-engine heavy bomber used extensively during World War II by the United States Army Air Force and the British Royal Air Force in all theaters of the war. The Consolidated Aircraft Company designed the B-24 in 1939, and one is now on display at the National Museum of the Mighty Eighth Air Force in Pooler, Georgia. An image of the B-24 Liberator is shown in Figure I.



© Commemorative Air Force/Scott Sloane

Figure I: Consolidated B-24 Liberator [i]

Detailed analyses of flight conditions during all sections of the specified mission profiles are discussed, that include cruise, climb, descent, take-off, landing, and combat maneuvers. All parameters found that act on the aircraft are calculated and compared using equations and guidance from federal regulations in 14 CFR § 25. The primary applied loads that act on an aircraft in flight are lift, drag, pressure loads, weight, and thrust.

Structural analyses of the B-24 fuselage during the highest loading scenario, a bombing run, are completed through beam bending, multi-cell web-longeron, circular and rectangular plate, cylindrical and stiffened shell analyses. Multi-cell web-longeron analysis is used to analyze the individual longerons and skin panels as part of an entire cohesive structure. Beam bending analysis approximates the fuselage as a beam with a singular cross section by means of smearing structural components. Circular plate analysis is used to analyze the frames in the fuselage, whereas rectangular plate analysis is used for the skin panels. Shell analysis analyzes the entire shape of the fuselage without individual structural members, and stiffened shell analysis adds in

the contribution of the internal components to the stiffness of the fuselage. Analyses produce values for stress that are compared against the yield strength of aluminum to determine the first failure location. The analyses are also performed for a damaged case, after the first locations have already failed. Failure locations and load factors for each analysis are shown in Figure II.

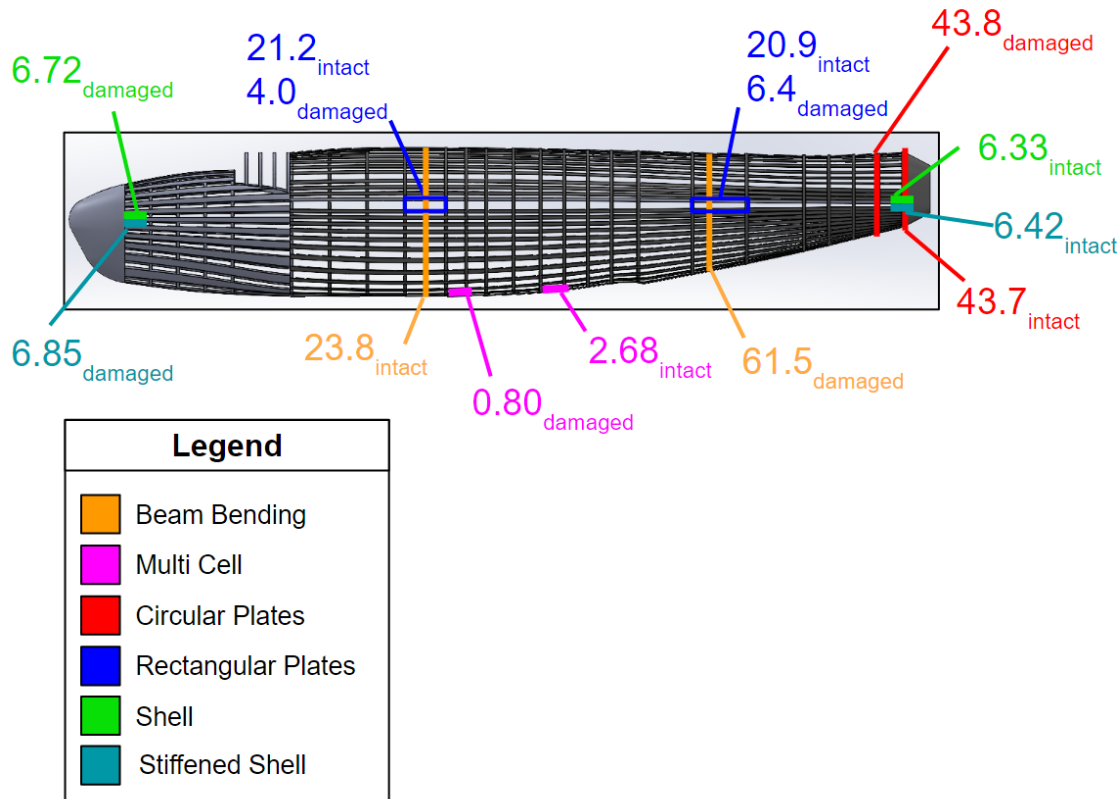


Figure II: Failure Locations and Load Factors for Each Analysis

Overall, the analyses suggest a location of failure close to the center of the fuselage. This location is expected because the payload and wings are mounted nearby. Some of the load factors do not correspond perfectly, most likely a result of assumptions made in smearing components for analyses that do not consider individual components. The group places the most trust in the multi-cell web-longeron analysis because the load factors are most in line with the expected magnitude, and this analysis is capable of analyzing individual longerons and skin panels as a cohesive system. The stiffened shell method is also capable of analyzing a cohesive system. The locations of failure for stiffened shell analysis reduce the group's trust in this method, because no loads are applied at the locations of failure to cause stress.

Table of Contents

1.0 Introduction	1
2.0 History of the Consolidated B-24 Liberator and Lindell Hendrix	1
3.0 Applied Aerodynamic Loading on the B-24 Liberator's Fuselage	3
3.1 Description of Applied Loads	3
4.2 Equations and Results	3
3.3 Validation of MATLAB	4
3.4 Selection of Worst-Case Loading Condition and Results	4
4.0 Beam Bending Analysis of the B-24 Fuselage During Bombing	5
4.1 Analysis Procedure	6
4.2 Analysis Results	8
4.3 MATLAB Validation	10
5.0 Multi-Cell Web-Longeron Analysis of the B-24 Fuselage During Bombing	10
5.1 Intact Procedure	11
5.2 Intact Results	13
5.3 Damaged Procedure	14
5.4 Damaged Results	14
5.5 MATLAB Validation	14
6.0 Plate Analysis of the Consolidated B-24 Fuselage During Bombing	15
6.1 Failure of Circular Plates Present in the Consolidated B-24 Liberator	15
6.1.1 Circular Plate Analysis Procedure	15
6.1.2 Intact and Damaged Results	16
6.2 Failure of Rectangular Plates Present in the Consolidated B-24 Liberator	17
6.2.2 Results	18
6.2.3 Rectangular Plate MATLAB Validation	19
7.0 Shell Analysis of the Consolidated B-24 Liberator Fuselage	19
7.1 Methodology	19
7.2 Results	21
7.3 MATLAB Validation	22
8.0 Stiffened Shell Analysis	22
8.1 Methodology	23
8.2 Results	24
8.3 MATLAB Validation	25
9.0 Conclusion	25
References	27
Appendix	30

List of Figures

Figure I: Consolidated B-24 Liberator in Flight	i
Figure II: Failure Locations and Load Factors for Each Analysis	ii
Figure 1: (a) 42-40506, Fightin' Sam [3] (b) First Lieutenant Lindell E. Hendrix with an F-105 [4]	2
Figure 2: Loading on B-24 Fuselage During Highest Loading Condition	4
Figure 3: Loading on B-24 Fuselage During the Remaining Loading Conditions	5
Figure 4: (a) B-24 Fuselage Structure (b) Simplified Model for Beam Bending Analysis	6
Figure 5: Vertical Displacement of the Fuselage	8
Figure 6: Longitudinal Displacement of the Fuselage	9
Figure 7: Effective Stress On the B-24 Liberator Fuselage	9
Figure 8: Geometry Models for Multi-Cell Web-Longeron Analysis (a) Cockpit (b) Aft (c) B-24 Fuselage Structure [18]	11
Figure 9: Moment Balance in z Direction	12
Figure 10: Force Balance of Shear Flows and Axial Force	12
Figure 11: Multi-Cell Web-Longeron Analysis in Intact Fuselage (a) Stress (b) Location	13
Figure 12: Multi-Cell Web-Longeron Analysis in Damaged Fuselage (a) Stress (b) Location	14
Figure 13: Multi-Cell Web-Longeron Validation Model	15
Figure 14: B-24 Fuselage Frame (a) CAD (b) Simplification	15
Figure 15: Stresses in Circular Frames	16
Figure 16: B-24 Skin Panels (a) CAD (b) Simplification	17
Figure 17: Stress in Rectangular Plate 1 (a) Intact (b) Damaged	18
Figure 18: (a) B-24 Fuselage Structure (b) Simplified Model for Shell Analysis	19
Figure 19: Effective Stress in the B-24 Fuselage Using Shell Analysis	22
Figure 20: (a) B-24 Fuselage Structure (b) Simplified Model for Stiffened Shell Analysis	23
Figure 21: Frame and Longeron Geometry	23
Figure 22: Effective Stress in the B-24 Fuselage Using Stiffened Shell Analysis	25
Figure 23: Failure Locations and Load Factors for Each Analysis	26

1.0 Introduction

The Consolidated B-24 Liberator entered service in 1941 as an alternative to the B-17 Flying Fortress and quickly became the most produced military aircraft in US history. The B-24 excelled in long-range precision bombing runs and was used widely in both theaters of World War II. First Lieutenant Lindell Hendrix piloted a B-24 and created unofficial safety protocols that were followed by other pilots of the aircraft. The structure of the B-24 is analyzed using beam bending, multi-cell web-longeron methods, circular and rectangular plate analyses as well as cylindrical and stiffened shell analyses. The following sections discuss likely failure locations and load factors for both intact and damaged configurations of the aircraft.

2.0 History of the Consolidated B-24 Liberator and Lindell Hendrix

The Consolidated B-24 Liberator was originally conceived to provide speed and range improvements over the B-17 Flying Fortress while also carrying a larger ordinance payload [1]. The main application of the B-24 Liberator was long-range missions to deliver large quantities of payload with high precision [1]. While the primary use of this aircraft was for precision bombing raids, the aircraft was also used to deliver supplies, such as in Operation Carpetbagger, where B-24 Liberators delivered supplies to French freedom fighters in preparation for D-Day. Over the course of World War II, 18,482 of these aircraft were produced, making it the single most produced aircraft in US military history [1].

The most common maneuvers for the B-24 Liberator were long-range endurance cruises when approaching and returning from long-range bombing missions, in addition to take-offs and landings. The lower service ceiling of the B-24, as opposed to the B-17, meant the B-24 was much more vulnerable to the anti-aircraft weaponry found in the European theater. The B-24 found its own in the Pacific theater because of its endurance capabilities over large expanses of the Pacific Ocean [2]. The B-24 housed at the National Museum of the Mighty Eighth Air Force, 42-40506, Fightin' Sam, was used extensively in Europe within the 801st special night Bombing Group from the 389th Bomb Group in the 8th Air Force. Fightin' Sam was painted black to better camouflage with the night sky, allowing covert resupply of resistance forces and deployment of ground forces. Fightin' Sam, and a B-24 pilot, First Lieutenant Lindell Hendrix, are shown in Figure 1.

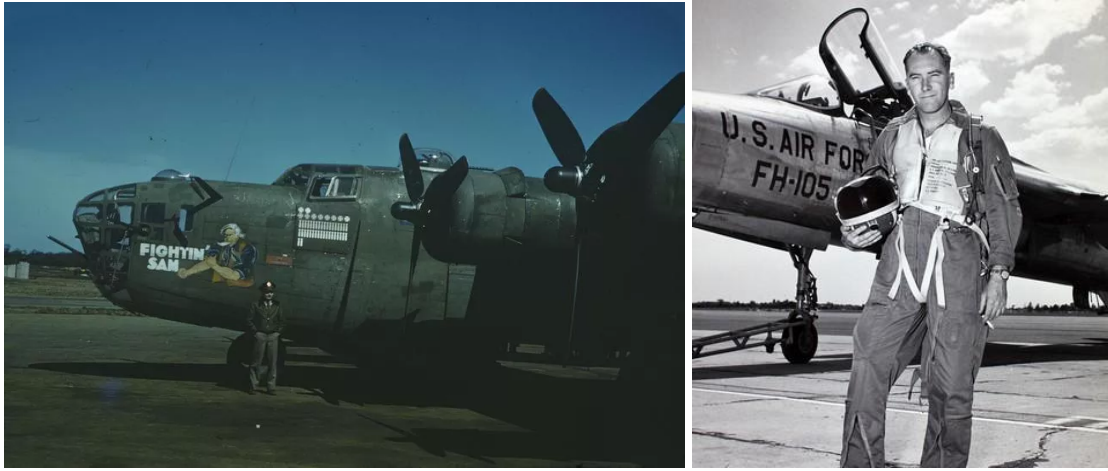


Figure 1: (a) 42-40506, Fightin' Sam [3] (b) First Lieutenant Lindell E. Hendrix with an F-105 [4]

First Lieutenant Lindell Eugene Hendrix was born in Illinois on March 7th, 1921. From childhood, Hendrix had an enthusiasm for aviation. After attending university for two years studying both chemistry and journalism, Hendrix took his experiences to the Air Cadet Academy in 1939, just a month into the war in Europe. He enlisted in the Army Air Corps soon after [5].

First Lieutenant Hendrix was deployed with the 491st Bombardment Group contained within the Eighth Air Force [6]. This detachment was stationed on the eastern coast of England. The 491st Bombardment Group flew solely Consolidated B-24 Liberators on bombing runs targeting crucial German infrastructure in France [7], then in support roles during Operation Market Garden and the campaign towards Berlin [8]. Hendrix introduced safety initiatives and performance reviews of the B-24, including a complete ban on smoking on board the aircraft, and a review of the aircraft's increased difficulty to control when heavily loaded [9]. Along with his entire unit, Hendrix received the Distinguished Unit Citation, for their role in a bombing raid on an oil refinery in Misburg, Germany [8]. Post World War II, First Lieutenant Lindell Hendrix served in various groups and attachments, including Aerial Photography, Intelligence, and the 51st Fighter Group [10].

First Lieutenant Hendrix was discharged in 1950, becoming a distinguished test pilot for Republic Aviation [10]. During his time at Republic Aviation, Hendrix most notably flew the P-47 Thunderbolt and the F-105 Thunderchief [11]. First Lieutenant Hendrix also became a freelance writer [10], notably with a published work discussing flutter, that appears in an issue of

the United States Air Force Aviation Safety Magazine [12]. First Lieutenant Lindell Hendrix died in San Diego, California on April 28th, 1980.

3.0 Applied Aerodynamic Loading on the B-24 Liberator's Fuselage

To properly determine the failure of an aircraft's fuselage, the applied loading that the fuselage is subjected to must be understood. Aerodynamic forces generated from the wings and stabilizers are transferred to the fuselage of aircraft. The fuselage of any aircraft also carries pressure, gust, and landing gear loads. All loads on a fuselage are calculated using equations and guidance from 14 CFR § 25. The calculation of applied loading under four different scenarios, climb, cruise, descent/landing, and a combat maneuver allows for the selection of the highest loading scenario. The combat maneuver selected for the B-24 is the deliverance of a full load of ordinance. Bombing release is determined to be the worst case loading scenario because of a high freestream velocity, inertial forces, and moderate air density. Calculations were performed in MATLAB and validated by hand. The largest error was 0.28% for the pitching moment. Applied loads on the B-24 fuselage are affected by atmospheric conditions and maneuvers. A description of loads carried by the fuselage, equations, results, and validation of MATLAB calculations are discussed.

3.1 Description of Applied Loads

Loads transferred from the wings to the fuselage include lift, drag, their respective bending moments, pitching moment, and engine thrust and torque. Lift and drag are distributed linearly along the wing-fuselage interface, the bending moments are about their neutral axes, and the pitching moment is about the quarter chord location. The B-24 uses an H-tail configuration, so loads from the vertical stabilizers are transferred to the fuselage through the horizontal stabilizer.

4.2 Equations and Results

There are various equations that are required to calculate loads. Equation 1 is used to calculate the lift of the wings and stabilizers.

$$L = C_L \frac{\rho V^2}{2} A \quad (1)$$

Where L is lift, ρ is air density, V is velocity, C_L is coefficient of lift, and A is planform area. Equation 2 is used to calculate the drag on the wings and stabilizers.

$$D = C_D \frac{\rho V^2}{2} A \quad (2)$$

Where D is drag and C_D is coefficient of drag. Equation 3 is used to calculate the pitching moment on the wings and stabilizers.

$$M_p = C_M \frac{\rho V^2}{2} Ac \quad (3)$$

Where M_p is pitching moment, C_M is coefficient of moment, and c is chord. Pressure loading on the fuselage is calculated using Equation 4.

$$P(\theta) = P_a + \frac{1}{2} \rho \left[U^2 - \left(\frac{\Gamma(\beta, \theta)}{2\pi r(\theta)} \right)^2 - \frac{2U\Gamma(\beta, \theta)}{\pi r(\theta)} \sin\theta - 4U^2 \sin^2\theta \right] \quad (4)$$

Where U is free stream velocity, θ and r are the position around the fuselage. Equation 5 is used to calculate $\Gamma(\beta, \theta)$, a component of Equation 4.

$$\Gamma(\beta, \theta) = 4\pi Ur(\theta) \sin(\beta) \quad (5)$$

3.3 Validation of MATLAB

MATLAB is used to calculate applied aerodynamic loading. Validation is performed by hand, using the equations in Section 3.2. The largest error was 0.28% for the pitching moment, this is within the acceptable error limit of 5%.

3.4 Selection of Worst-Case Loading Condition and Results

Based on calculations, loading on the B-24 is highest during a bombing maneuver. High velocity, large payload, and atmospheric density cause the highest loading. All future analyses will be evaluated at the loading present in this scenario. The results are shown in Figure 2.

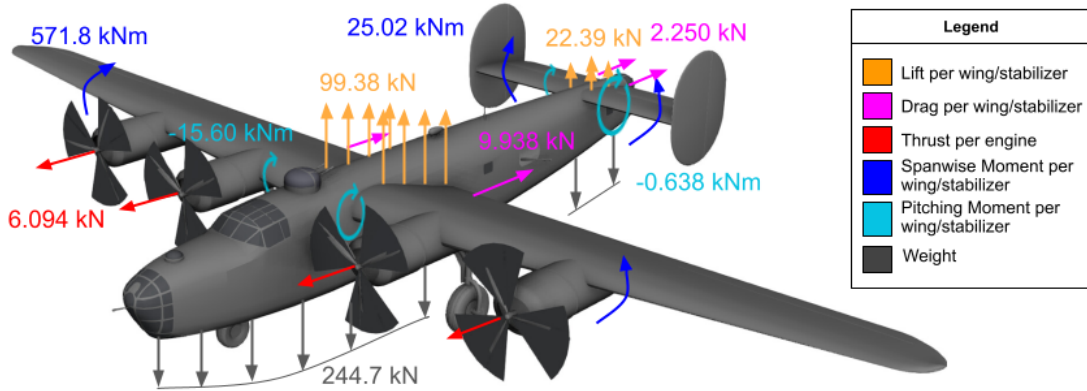


Figure 2: Loading on B-24 Fuselage During Highest Loading Condition [14]

The weight shown includes the weight of the payload. Landing gear loads are not shown because the aircraft is in flight. The aircraft is unpressurized and the net pressure loading is

approximately zero. Maximum pressure loading on the bottom of the fuselage is 61.54 kPa. Figure 3 showcases the other three loading conditions.

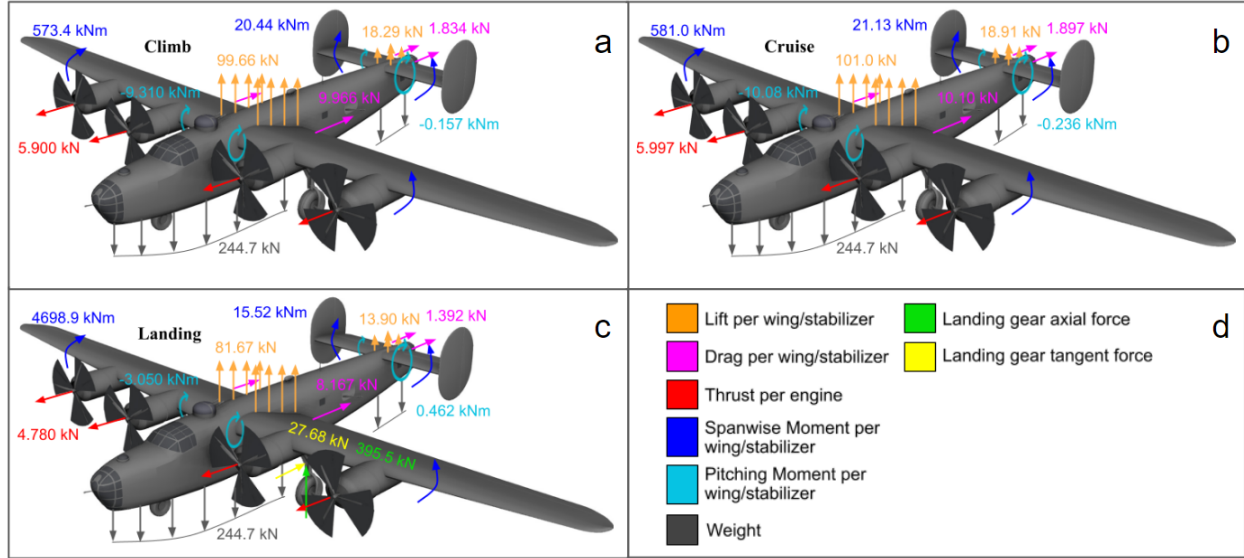


Figure 3: Loading on B-24 Fuselage During the Remaining Loading Conditions: a) Climb, b) Cruise, c) Landing, d) Legend [14]

4.0 Beam Bending Analysis of the B-24 Fuselage During Bombing

One way to analyze the structural integrity of a fuselage is through beam bending analysis, where the structure is approximated as a beam with various distributed loads applied along the length. For this method, four different partial differential equations of motion are solved using Galerkin's method. Based on the fuselage geometry and the applied distributed loads the displacement of the fuselage is determined numerically, that is then used to calculate the effective stress along the entire fuselage. Effective stress and material yield strength are then compared to determine the potential locations of failure and applicable structural safety factors in this loading scenario. Beam bending analysis is completed for a bombing maneuver at 16,000 ft and an airspeed velocity of 135 m/s, for both intact and damaged conditions. Analysis was completed in MATLAB and compared with found test data, where the error was 6.10 %. The structure of the B-24 fuselage, along with a simplified version for analysis, is shown in Figure 4.

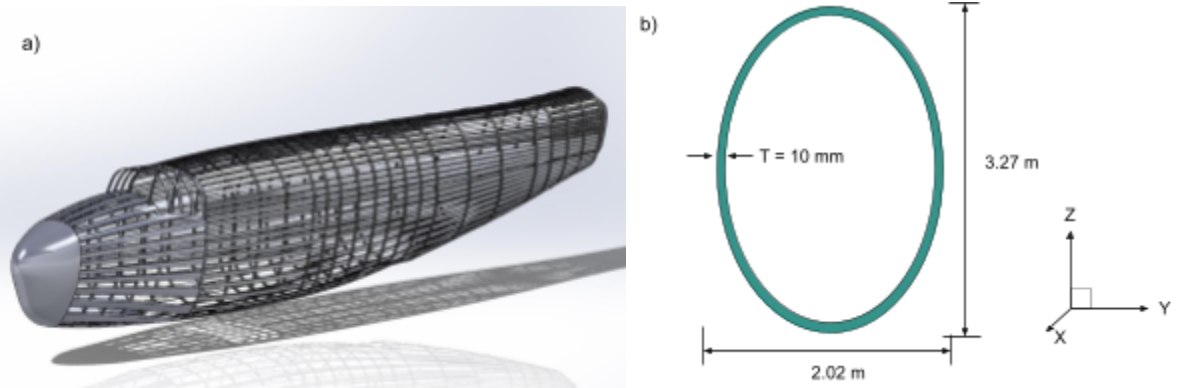


Figure 4: (a) B-24 Fuselage Structure (b) Simplified Model for Beam Bending Analysis

The following sections detail the procedure and results for an intact and damaged fuselage.

4.1 Analysis Procedure

The structure of the fuselage was simplified for beam bending analysis, shown in Figure 5, with an effective skin thickness of 10 mm. Geometric constants must first be calculated, including the area, moment of inertia, and polar moment of inertia. The standard equations for each are applied. The specific loading scenario of this maneuver only has axial displacement in the x-direction and bending displacement in the z-direction. The governing equation for the x-direction is Equation 6.

$$\rho A \frac{\partial^2 u(x,t)}{\partial t^2} - EA \frac{\partial^2 u(x,t)}{\partial x^2} = f_x(x, t) \quad (6)$$

Where ρ is the density, A is the cross-sectional area, E is Young's modulus of the fuselage, $u(x, t)$ is the displacement in the x-direction, and $f_x(x, t)$ is the applied loads in the x-direction.

The governing equation for the z-direction is Equation 7.

$$\rho A \frac{\partial^2 w(x,t)}{\partial t^2} + EI_{yy} \frac{\partial^4 w(x,t)}{\partial x^4} = f_z(x, t) \quad (7)$$

To solve Equation 6 and Equation 7 in both time and space, a separable series solution is assumed in the form of Equation 8.

$$w(x, t) = \sum_{n=1}^{N} X_n(x) T_n(t) \quad (8)$$

Where N is the number of mode shapes used to approximate the response of the beam and can be a different value in Equations (6) and (7). Once Equation 8 is substituted into the governing equations, the series is expanded to N terms. Following this substitution, the expanded form of

the governing equation is individually multiplied by each mode shape of interest and then integrated along the length of the fuselage. The mode shapes for free-free boundary conditions were used in this scenario. The free-free longitudinal displacement mode shapes are generated with Equation 9.

$$U_n(x) = \cos\left(\frac{n\pi x}{L}\right) \quad (9)$$

Where n is the number of the mode, x is the position along the fuselage, and L is the length of the fuselage. The mode shapes for transverse bending with free-free boundary conditions (excluding rigid body modes, $m = 0, 1$) are given by Equations 10 and 12.

$$X(x) = \cos \gamma_1 \left(\frac{x}{L} - \frac{1}{2} \right) - \frac{\sin(\gamma_1/2)}{\sinh(\gamma_1/2)} \cosh \gamma_1 \left(\frac{x}{L} - \frac{1}{2} \right) \quad (10)$$

Where Equation 10 is valid for even modes and γ_1 is calculated as the m^{th} root of Equation 11.

$$\tan\left(\frac{\gamma_1}{2}\right) + \tanh\left(\frac{\gamma_1}{2}\right) = 0 \quad (11)$$

$$X(x) = \sin \gamma_2 \left(\frac{x}{L} - \frac{1}{2} \right) + \frac{\sin(\gamma_2/2)}{\sinh(\gamma_2/2)} \sinh \gamma_2 \left(\frac{x}{L} - \frac{1}{2} \right) \quad (12)$$

$$\tan\left(\frac{\gamma_2}{2}\right) + \tanh\left(\frac{\gamma_2}{2}\right) = 0 \quad (13)$$

Where γ_2 is the m^{th} root of Equation 13. The analysis is performed multiple times for each governing equation while incrementally increasing the number of mode shapes until the solution converges to a 2% difference between the current and previous iteration. Then, the resulting ordinary differential equation was solved in the time domain and the full structural displacement response was determined. To calculate the strain in the x-direction Equation 14 was used.

$$\varepsilon_x = \frac{\partial u}{\partial x} - z \frac{\partial^2 w}{\partial x^2} \quad (14)$$

Where ε_x is the strain in the x-direction, u is the displacement in the x-direction, z is the distance from the neutral axis, and w is the displacement in the z-direction. Equation 15 was used to calculate the shear strain in the xz-plane.

$$\gamma_{xz} = -2z \frac{\partial^2 w}{\partial x \partial z} \quad (15)$$

Where γ_{xz} is the strain in the xz-plane, z is the distance from the neutral axis, and w is the displacement in the z-direction. Stress in the x-direction is calculated with Equation 16.

$$\sigma_x = E \varepsilon_x \frac{1}{1-v^2} \quad (16)$$

Where E is the Young's Modulus of the fuselage material, ε is the calculated strain, and v is the Poisson's ratio of the fuselage material. Von Mises failure criterion was then used to evaluate for failure, as shown in Equation 17.

$$\sigma_{effective} = \sqrt{\sigma_x^2 + 3(\tau_{xz})^2} \geq \sigma_{yield} \quad (17)$$

Where $\sigma_{effective}$ is the effective stress on the fuselage and σ_{yield} is the yield strength of the fuselage material.

4.2 Analysis Results

Displacement of the fuselage was only present in the x and z directions of the fuselage because the y and θ directions have zero net applied loads. The displacement of the fuselage in the z direction as a function of the fuselage station, x , is shown in Figure 5.

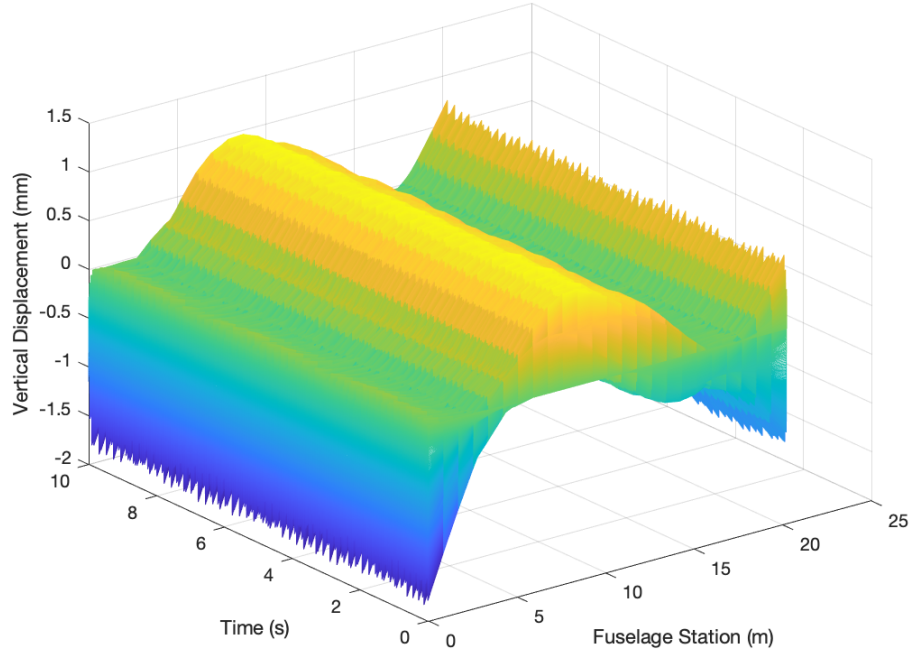


Figure 5: Vertical Displacement of the Fuselage

The longitudinal displacement of the fuselage is shown in Figure 6.

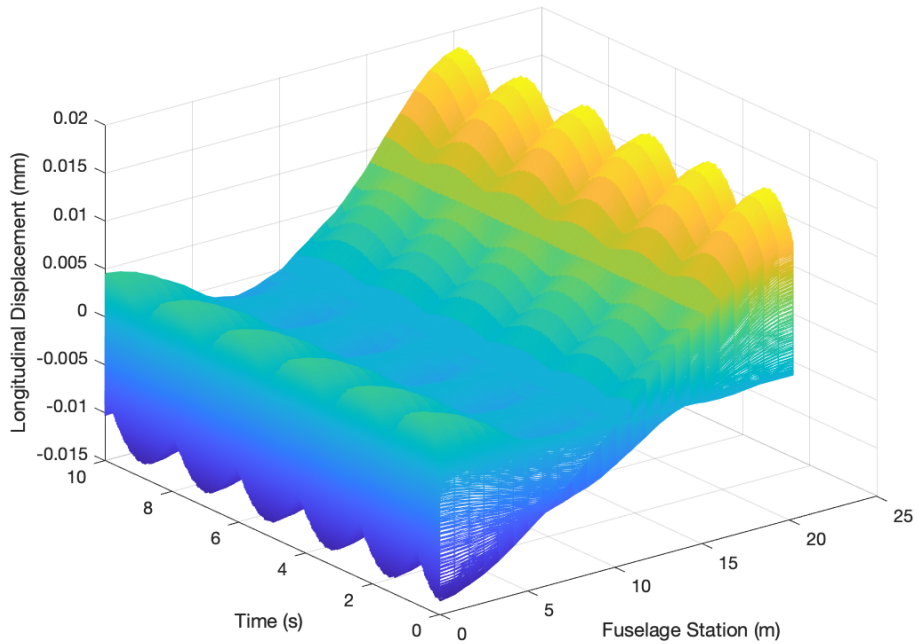


Figure 6: Longitudinal Displacement of the Fuselage

The effective stress for each fuselage station, as calculated from the data in Figure 5 and Figure 6, is shown in Figure 7.

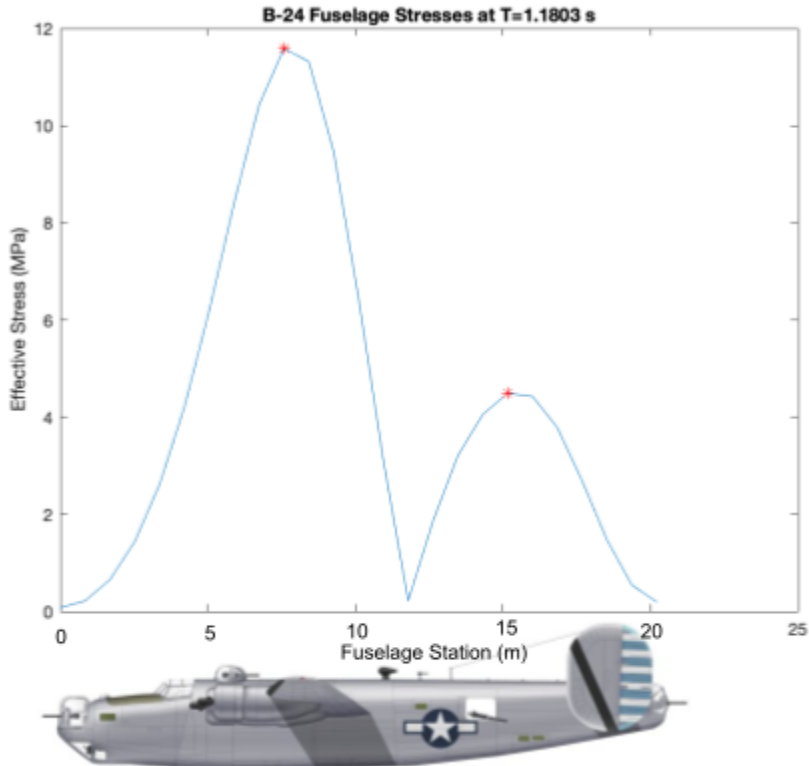


Figure 7: Effective Stress On the B-24 Liberator Fuselage [13]

The highest effective stress is found at an x position of 7.58 m along the fuselage and at 1.18 seconds into the analyzed time response of the structure. When compared to the yield strength of aluminum [15], the fuselage will fail at a load factor of 23.8. For the damaged case, the next highest effective stress peak at this time is found at an x position of 15.17 m along the fuselage. When compared to the yield strength of aluminum [16], the fuselage will begin to fail at this second location at a load factor of 61.5.

4.3 MATLAB Validation

Validation of the beam bending was performed by comparing it against experimental data [17]. The experimental case selected involved a cantilever beam loaded at the tip, which was also modeled in the beam bending MATLAB code. An error of 6.10 % was realized.

5.0 Multi-Cell Web-Longeron Analysis of the B-24 Fuselage During Bombing

Multi-cell web-longeron analysis is a method for analyzing semi-monocoque aircraft fuselages such as the B-24. Multi-cell web-longeron analysis involves the simplification of longerons into rods spanning the length of the fuselage that only carry axial stress and webs that carry shear stress. The calculated stresses obtained from the analysis are evaluated for failure using the Von Mises failure criterion. Von Mises compares the stress values in each longeron and web to the yield strength of 6061 aluminum. Where the calculated stress values exceed the yield strength of the material, yielding, and subsequent failure occurs. A load factor may be applied to the aircraft to reach the failure point. The multi-cell web-longeron analysis was completed for a bombing maneuver at 16,000 ft at a velocity of 135 m/s, for both intact and damaged conditions, whereupon the structure has already yielded in one location and is no longer load bearing. Analysis was completed in MATLAB using code that was validated using hand calculations on a simplified geometry of 6 longerons and 7 webs, where the calculated error for a test model was 0%. Multi-cell web-longeron analysis requires the structure to be geometrically simplified into webs and longerons, shown in Figure 8 along with the true structure of the B-24 fuselage.

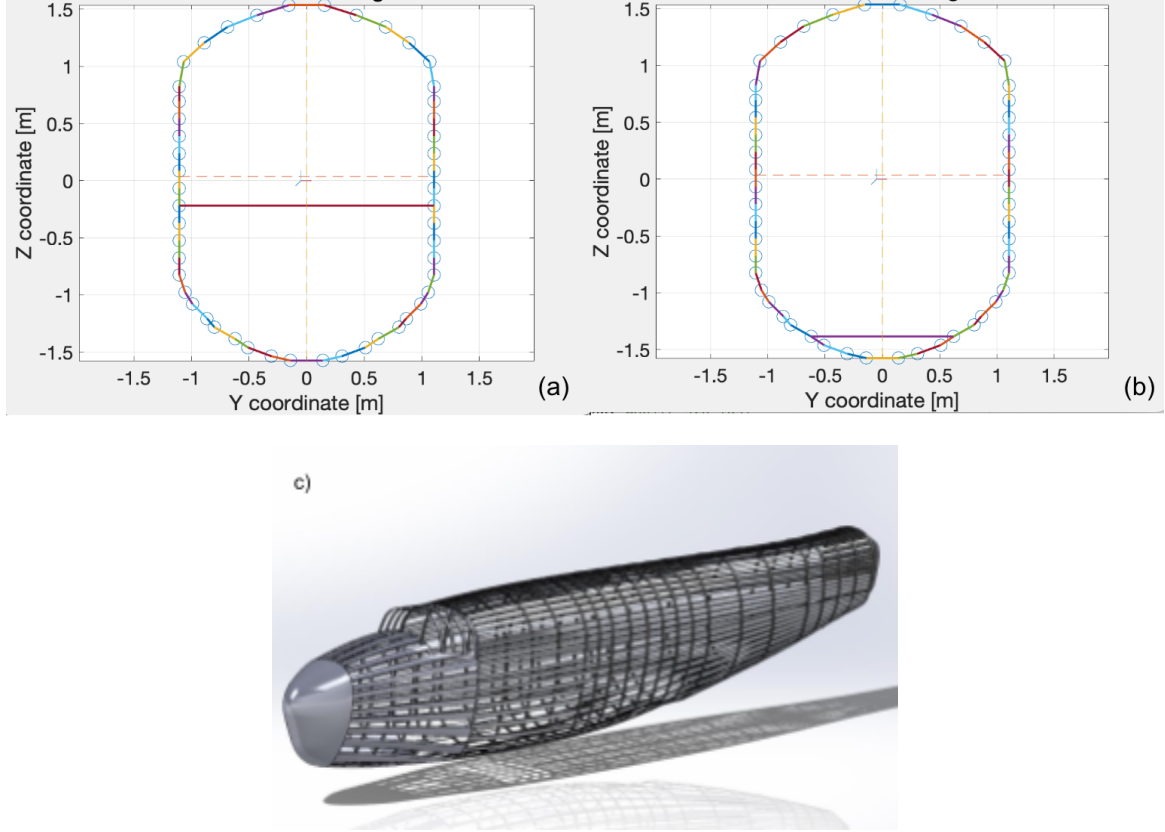


Figure 8: Geometry Models for Multi-Cell Web-Longeron Analysis (a) Cockpit (b) Fuselage (c) True Structure [18]

Two model geometries were used, one with a low-mounted floor, and another with a higher-mounted floor representing the cockpit. The two geometries were applied to match their respective locations along the fuselage. The following sections discuss the procedure and results for an intact and damaged fuselage.

5.1 Intact Procedure

Equation 18 was used to find the neutral axis of the fuselage for forces in the z -direction.

$$\bar{z} = \frac{\sum A_i z_i}{\sum A_i} \quad (18)$$

Where \bar{z} is the neutral axis, A_i is the longeron area, and z_i is the longeron distance from the datum. The effective areas of each longeron were found using Equation 19.

$$A_{eff} = A_{fi} + \Sigma \frac{bt}{6} \left(2 + \frac{z_{i+1}}{z_i} \right) \quad (19)$$

Where A_{eff} is the effective area of the longeron, A_{fi} is the flange area, b is the length of the adjacent web, t is the thickness of the adjacent web, and z is the distance from the neutral axis to the longeron. Equation 20 was used to find the ratios between the forces in each longeron.

$$\frac{F_1}{A_{eff_1} z_1} = \frac{F_n}{A_{eff_n} z_n} \quad (20)$$

Where F is the force in each longeron member. Equation 21 was used to find the force in each longeron in the z -direction.

$$\Sigma M = 0 = \Sigma F_n z_n - F_{applied} \quad (21)$$

Where $F_{applied}$ is the sum of forces in the z direction at the given station along the fuselage. Figure 9 shows a moment balance in the z -direction using Equation 21.

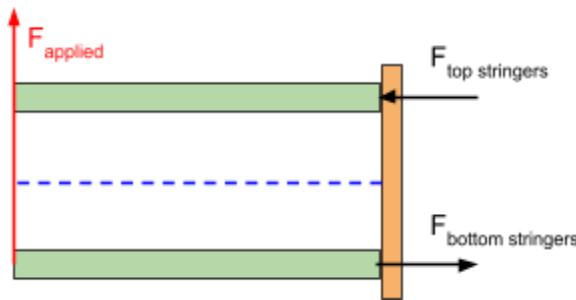


Figure 9: Moment Balance in z Direction

The steps in Section 5.1 were repeated in the y -direction, where each z in the equations is replaced by y . The total axial force in each longeron was found by adding the forces that result from loading in both the y and z directions. The force in each longeron and adjacent web were balanced using Equation 22.

$$F_i + q_{i-1} = q_i \quad (22)$$

Where q is the shear flow in a web. The force balance from Equation 23 is shown in Figure 10.

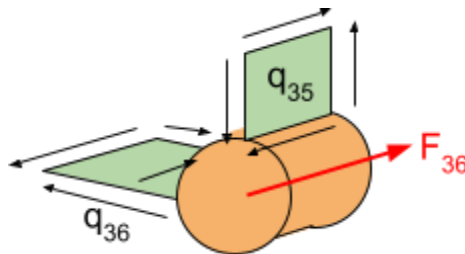


Figure 10: Force Balance of Shear Flows and Axial Force

Equation 23 is used to balance any applied torques in the fuselage with the shear flows.

$$T = \sum_{i=1}^n 2\bar{A}_i q_i \quad (23)$$

Where \bar{A} is the area enclosed by a web and the reference longeron, q_i is the shear flow in the web, and T is the sum of torque in the fuselage. The moments were calculated about the geometric center of the fuselage. Equation 24 imposes compatibility between the cells using angle of twist.

$$\theta = \sum_{i=1}^n \frac{q_i s_i}{2\bar{A}Gt_i} \quad (24)$$

Where s_i is the length of the web, and G is the shear modulus. The standard stress equations were used to calculate axial and shear stresses in the longerons and webs. The stresses in each web and longeron are compared to the yield strength of aluminum using the Von Mises criterion. The entire procedure is repeated at multiple stations along the fuselage to determine the location of the first failure.

5.2 Intact Results

The analysis was performed for multiple stations along the fuselage, but the cross-section with the highest stress value, at the 10.95 m station, is shown for ease of viewing. Figure 11 shows the stresses in the intact fuselage.

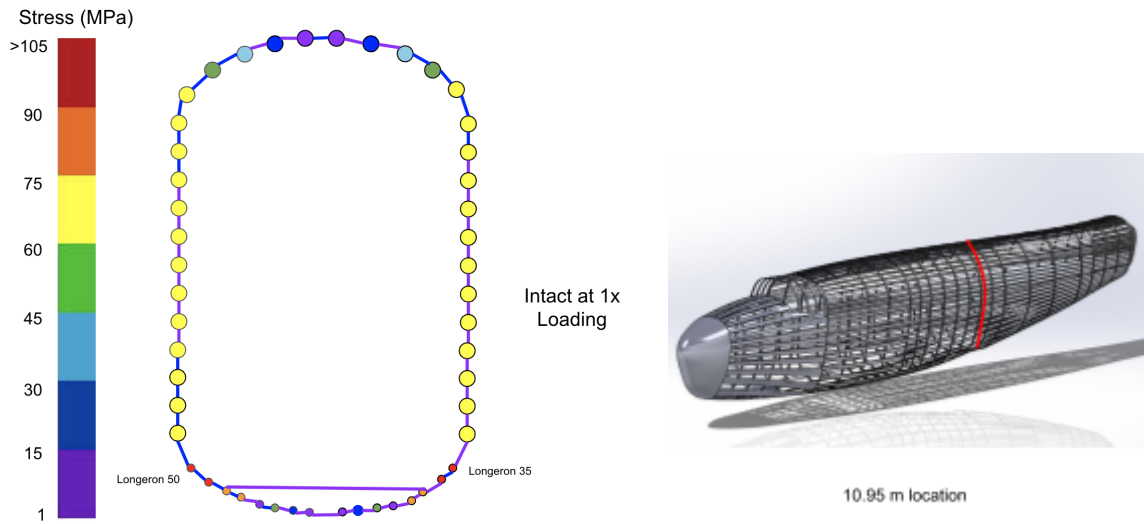


Figure 11: Multi-Cell Web-Longeron Analysis in Intact Fuselage (a) Stress (b) Location

According to the multi-cell web-longeron analysis for an intact fuselage, shown in Figure 16, longerons 35, and 50 had the highest reported stresses of 103.3 MPa compared to the yield strength of aluminum, 276 MPa [16]. Longerons 35 and 50 would fail at a loading factor of 2.675.

5.3 Damaged Procedure

The procedure for multi-cell web-longeron analysis for a damaged fuselage is similar to the intact state. Longerons 35 and 50 were removed from the model to conduct the analysis in a damaged state.

5.4 Damaged Results

With the initially failed components removed from the model, Figure 12 shows the stresses at station 8.9 m, where the new highest stress is found.

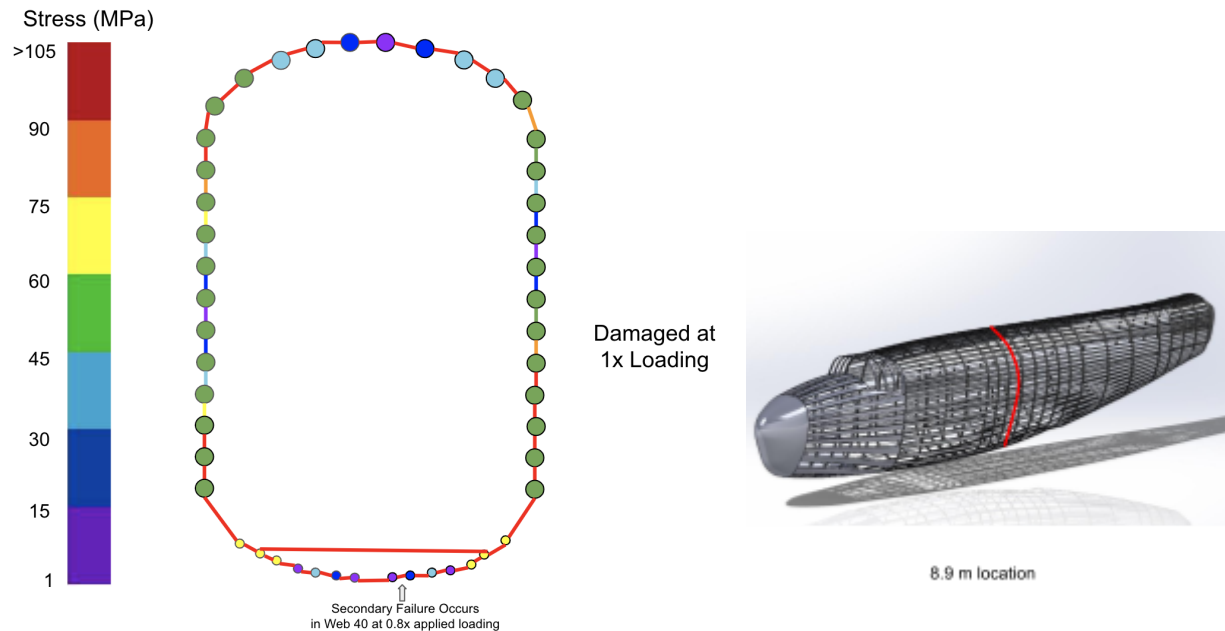


Figure 12: Multi-Cell Web-Longeron Analysis in Damaged Fuselage (a) Stress (b) Location

The next location the damaged fuselage would fail is in web 40, at a loading factor of 0.8, meaning the failure of the first longerons is catastrophic to the structure of the fuselage.

5.5 MATLAB Validation

Validation of the multi-cell web-longeron analysis was performed by giving the produced MATLAB script a simplified geometry, and comparing results from the MATLAB code output to that of hand calculations, with the model used shown in Figure 13, where a lift force applied at a

unit distance of 1000 N was applied.

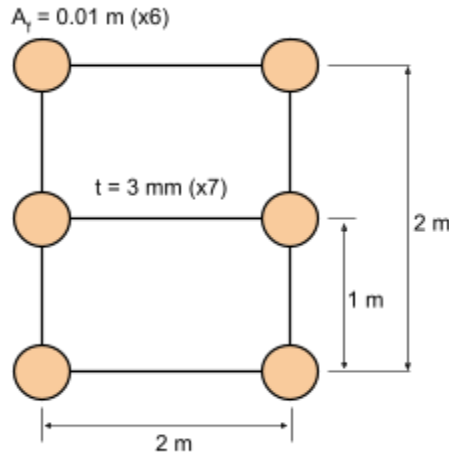


Figure 13: Multi-Cell Web-Longeron Validation Model

Exact stresses for each structural component were obtained, producing an error of 0%.

6.0 Plate Analysis of the Consolidated B-24 Fuselage During Bombing

Directly applied to the Consolidated B-24, plate analyses provide an understanding of where failures in fuselage frames and skin panels occur. Circular plate analysis was performed by approximating the frames as annular circular plates, and the first failure occurred at 43.79x loading. For rectangular plate analysis, skin panels were approximated as a rectangle, and the first failure occurred at 12.2x loading. A validation error of 25.8% was realized for this analysis.

6.1 Failure of Circular Plates Present in the Consolidated B-24 Liberator

The following sections detail circular plate analysis of B-24 frames that are shown in Figure 14.

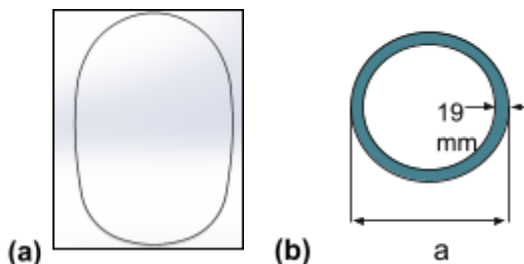


Figure 14: B-24 Fuselage Frame (a) CAD (b) Simplification

Where a varies along the length of the fuselage, and each frame is 0.0190 m thick.

6.1.1 Circular Plate Analysis Procedure

Equation 25 was used to find the flexural rigidity of a circular plate.

$$D = \frac{ET^3}{12(1-v^2)} \quad (25)$$

Where E is the Young's modulus of 6061 Aluminum that has a value of 70 GPa, T is the thickness of the plate, and v is the Poisson's ratio of aluminum, 0.3, following a governing assumption for circular plate theory in metals. The B-24's frames consist of concentric rings making a hollow interior, meaning Case 5, that contains a hollow center with edge-applied moments, is the most relevant for this application. Equation 26 calculates the displacement of the plate w , when the edge is simply supported and internal and external moments are applied.

$$w = C_1 \frac{r^2}{4} + C_2 \ln\left(\frac{r}{a}\right) + C_3 \quad (26)$$

Where r is the inner radius of the plate, a is the outer radius of the plate, and C_1 , C_2 , and C_3 , are constants and are calculated using formulas 27 through 29. Equation 27 calculates C_1 .

$$C_1 = \frac{2(M_2 a^2 - M_1 b^2)}{(1+v)(a^2 - b^2) D} \quad (27)$$

Where M_2 is the outer edge moment and M_1 is the inside edge moment. Equation 28 calculates C_2 .

$$C_2 = \frac{-a^2 b^2 (M_2 - M_1)}{(1+v)(a^2 - b^2) D} \quad (28)$$

Equation 29 calculates C_3 from C_1 .

$$C_3 = \frac{-C_1 a^2}{4} \quad (29)$$

Stress is calculated using the first and second derivatives of displacement.

6.1.2 Intact and Damaged Results

The results of the circular plate analysis of intact frames are shown in Figure 15.

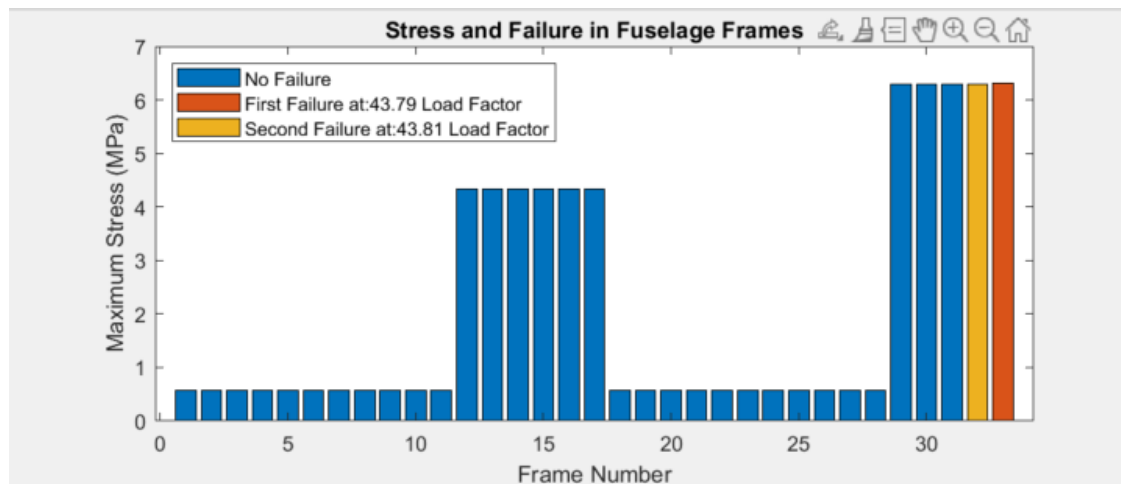


Figure 15: Stresses in Circular Frames

Failure occurred in frame 33 at a load factor of 43.79. To simulate a damaged condition, the procedure in Section 3.1 was followed with increased moment loading until failure of a second frame. The second failure occurred in frame 32 at a load factor of 43.81.

6.2 Failure of Rectangular Plates Present in the Consolidated B-24 Liberator

The following sections detail rectangular plate analysis of applicable fuselage components. In the Consolidated B-24 Liberator, the sections of fuselage skin between each pair of adjacent frames and longerons is approximated as rectangular plates. An example of a panel and its representative rectangular model are shown in Figure 16.



Figure 16: B-24 Skin Panels (a) CAD (b) Simplification

Two panels were selected for analysis based on the locations of the fuselage with the highest stress in the beam bending analysis previously performed on the B-24.

6.2.1 Procedure

The first step of solving the plates is to derive the governing equations for the plate. Equation 30 is the equilibrium equation for the plate in the z-direction.

$$\frac{\partial Q_x}{\partial x} + \frac{\partial Q_y}{\partial y} + \frac{\partial}{\partial x} \left(N_x \frac{\partial w}{\partial x} \right) + \frac{\partial}{\partial y} \left(N_y \frac{\partial w}{\partial y} \right) + \frac{\partial}{\partial x} \left(N_{xy} \frac{\partial w}{\partial y} \right) + \frac{\partial}{\partial y} \left(N_{xy} \frac{\partial w}{\partial x} \right) + q = \rho \frac{\partial^2 w}{\partial t^2} \quad (30)$$

Where q is the applied transverse loading, and ρ is the density. To solve Equation 30, the separable solution form in Equation 31 is assumed.

$$w(x, y, t) = X(x)Y(y)T(t) \quad (31)$$

Where $X(x)$ and $Y(y)$ are the spatial components of the solution and $T(t)$ is the temporal solution. Next, trial functions for the spatial component are selected based on the boundary conditions of the plate. Since panels are riveted to the fuselage, simply supported boundary conditions are assumed in both the x and y directions. Equation 32 is the trial function used.

$$X(x) = \sin\left(\frac{(m-1)\pi x}{a}\right) \quad (32)$$

Where m is the number of the trial function and a is the length of the plate in the axis of the spatial component of interest. Next, each combination of possible trial functions is multiplied

together to generate mode shapes that are then sorted by natural frequency. Now, Galerkin's method is applied to remove the spatial component, and the resulting ODE is solved in time for the temporal solution. Next, the time and space solutions are combined to find the displacement of the plate. With the displacement calculated, the stresses and strains in the plate are calculated and Von Mises failure criterion is evaluated with Equation 33.

$$\sigma_{eff} = \sqrt{\sigma_x^2 + (\sigma_x - \sigma_y)^2 + \sigma_y^2 + 3\tau_{xy}^2} \quad (33)$$

To represent a damaged condition, boundary conditions, and dimensions are changed to add a free edge, representing a split plate. Equation 34 is the trial function used for the simple-free boundary conditions of the plate.

$$X(x) = \sin\left(\gamma_2\left(\frac{x}{2a} - \frac{1}{2}\right)\right) + \frac{\sin(\gamma_2/2)}{\sinh(\gamma_2/2)} \sinh\left(\gamma_2\left(\frac{x}{2a} - \frac{1}{2}\right)\right) \quad (34)$$

Where a is the length of the plate in the axis of interest and γ_2 is the roots of Equation 35.

$$\tan\left(\frac{\gamma_2}{2}\right) + \tanh\left(\frac{\gamma_2}{2}\right) = 0 \quad (35)$$

The procedure for intact rectangular plates is now repeated under the new conditions.

6.2.2 Results

For the intact case, plate 1 failed first at a load factor of 21.2x loading when intact, and then plate 2 would fail shortly after at 20.9x loading. For the damaged case, the first failure occurred at plate 1 at a load factor of 4.0x loading, followed by a failure at plate 2 at a load factor of 6.4x loading. The effective stresses of the intact and damaged rectangular plate analyses on plate 1 are shown in Figure 17.

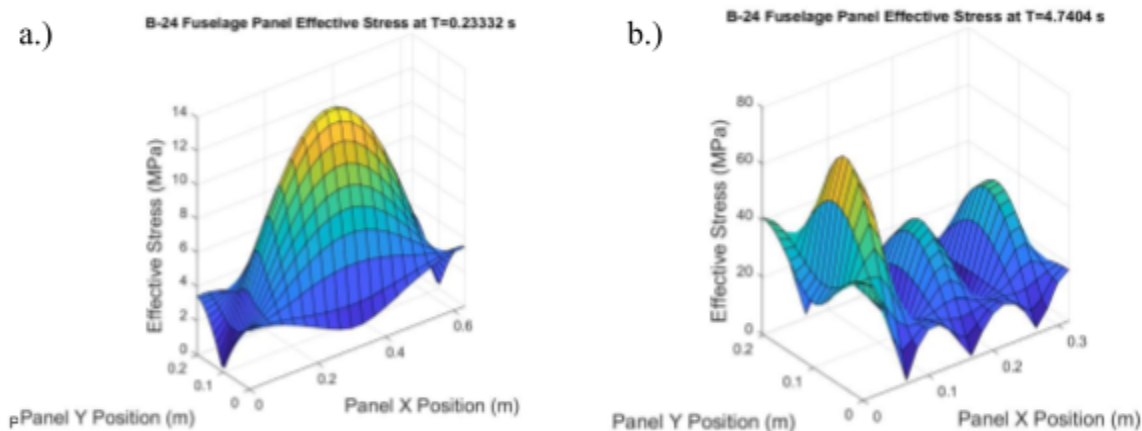


Figure 17: Stress in Rectangular Plate 1 (a) Intact (b) Damaged

6.2.3 Rectangular Plate MATLAB Validation

Validation of the rectangular plate analysis was performed by comparing experimental data to the results from the MATLAB script [19]. The experimental data was from an aluminum 0.5994 m square plate with a thickness of 1.397 mm, subjected to lateral pressure loading. An error of 25.8% was realized. While this error is large, the resulting errors possibly arise from variations in the true material properties of the aluminum compared to the values that were used for analysis.

7.0 Shell Analysis of the Consolidated B-24 Liberator Fuselage

Directly applied to the Consolidated B-24, a shell analysis provides an understanding of where failures in the fuselage occur. An unstiffened shell analysis was performed by approximating the fuselage as a hollow cylinder. The analysis of this hollow cylinder showed the first failure occurred at 6.33x loading at 20.22 m along the fuselage 136.5 degrees from the top centerline on the port side of the fuselage. The second failure occurred at 6.72x applied loading at the 20.22 m station in the same circumferential location as the first failure point on the starboard side of the fuselage. The following sections detail the methodology, results, and validation of the shell analysis. The true geometry and simplified geometry for the shell method is shown in Figure 18.

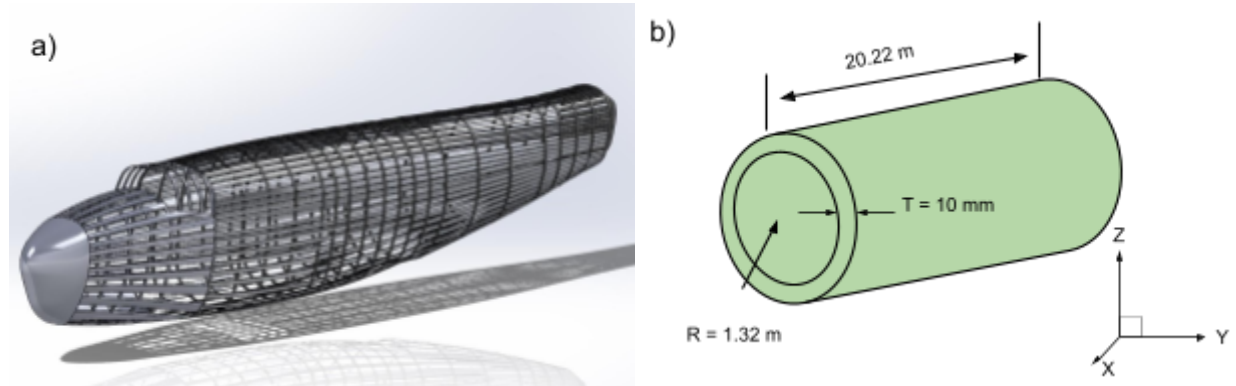


Figure 18: (a) B-24 Fuselage Structure (b) Simplified Model for Shell Analysis

The following sections detail the methodology, results, and validation of shell analysis.

7.1 Methodology

The first step to shell analysis is to apply thin circular cylindrical shell theory to the general theory. The equations of motion are shown in Equations 36 to 38.

$$q_\alpha \frac{R^2(v^2-1)}{Eh} = \frac{\partial^2 u}{\partial s^2} + \frac{1-v}{2} \frac{\partial^2 u}{\partial \theta^2} + \frac{1+v}{2} \frac{\partial^2 v}{\partial \theta \partial s} + v \frac{\partial}{\partial s} - \frac{h}{2R} \frac{\partial^3 w}{\partial \theta^2 \partial s^3} - \frac{h}{2R} \frac{\partial^3 w}{\partial s^3} \quad (36)$$

$$\left(q_\beta + \frac{1}{R}m_\alpha\right) \frac{R^2(v^2-1)}{Eh} = \frac{1+v}{2} \frac{\partial^2 u}{\partial \theta \partial s} + \frac{1-v}{2} \frac{\partial^2 v}{\partial s^2} + \frac{\partial^2 v}{\partial \theta^2} + \frac{\partial w}{\partial \theta} - \frac{h}{2R} \left(1 + \frac{h}{6R}\right) \frac{\partial^3 w}{\partial \theta^3} - \frac{h}{2R} \left(1 + \frac{h}{6h}\right) \frac{\partial^3 w}{\partial \theta \partial s^2} \quad (37)$$

$$-q_n \frac{R^2(v^2-1)}{Eh} = v \frac{\partial u}{\partial s} + \frac{\partial v}{\partial \theta} + w + k\nabla^4 - \frac{h}{2R} \frac{d^2 w}{d\theta^2} - \frac{hv}{2R} \frac{\partial^2 w}{\partial s^2} \quad (38)$$

where E is the young's modulus of 6061 aluminum, v is poisson's ratio, h is the shell skin thickness, q_n , q_a , and q_b are the applied loads in the normal, alpha and beta directions respectively. m_α is the applied moment in the alpha direction. K represents a computed constant relating skin thickness to radius of the fuselage, and w is the displacement in the z direction.

A fuselage is a finite-length shell with shear diaphragm boundary conditions, as shown in Equation 36.

$$w = M_x = N_x = v = 0 \quad \text{at } x = 0, l \quad (39)$$

A separable solution form is assumed, shown in Equation 40.

$$w(s, \theta, t) = S(s)\Theta(\theta)T(t) \quad (40)$$

Where $S(s)$ and $\Theta(\theta)$ are the spatial components of the solution and $T(t)$ is the temporal solution. The mode shapes in the u direction are given by Equation 41.

$$u = A(t) \cos \lambda s \cos n\theta \quad (41)$$

The mode shapes in the v direction are given by Equation 42.

$$v = B(t) \sin \lambda s \sin n\theta \quad (42)$$

The mode shapes in the normal direction are given by Equation 43.

$$w = C(t) \sin \lambda s \cos n\theta \quad (43)$$

Where λ is given by Equation 44.

$$\lambda = \frac{m\pi R}{l} \quad (44)$$

Where m is a positive integer, R is the radius of the shell, and l is the length of the fuselage. The mode shapes are sorted by natural frequency. Galerkin's method is applied to remove the spatial component, and the resulting ODE is solved in time. Next, the time and space solutions are combined to find the displacement of the shell. With the displacement calculated, the stresses and strains in the shell are calculated and the Von Mises failure criterion is evaluated with Equation 45.

$$\sigma_{eff} = \sqrt{\sigma_x^2 + (\sigma_x - \sigma_y)^2 + \sigma_y^2 + 3\tau_{xy}^2} \quad (45)$$

The analysis is repeated to find the second location of failure for a damaged case.

7.2 Results

For the intact case, the fuselage was found to first fail at a location 20.22 m along the fuselage 136.5 degrees from the top centerline of the port side of the fuselage at a loading factor of 6.33. The second failure occurs at a location 0 m along the fuselage at the same circumferential location on the starboard side and at a loading factor of 6.72. The stress in the fuselage is shown in Figure 19.

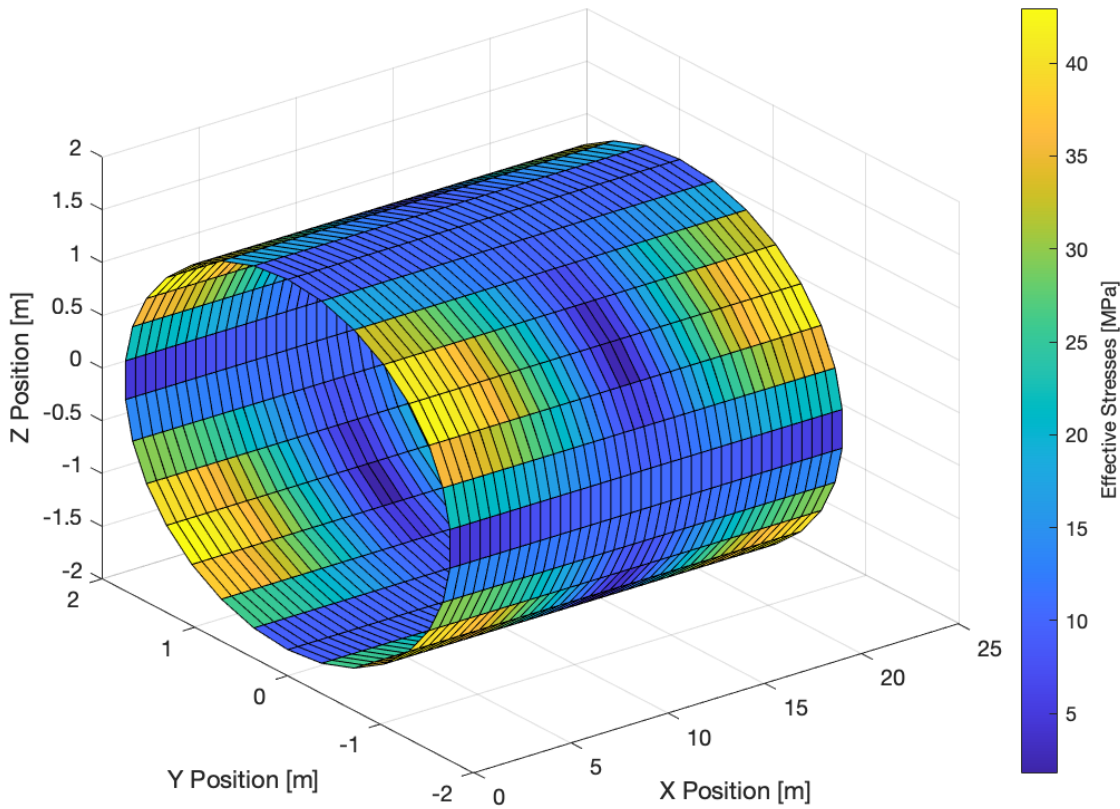


Figure 19: Effective Stress in the B-24 Fuselage Using Shell Analysis

7.3 MATLAB Validation

Validation of the basic shell analysis was performed by comparing it against experimental data [20]. The validation case applied combined compression and bending to a pressurized cylinder until failure occurs. Inputting the geometry from the empirical testing into the shell code, and comparing the output of the code and the empirical results produces an error of 9.16%.

8.0 Stiffened Shell Analysis

Stiffened shell analysis is a modification of shell analysis where individual components are not smeared and are considered in the analysis as stiffeners to the overall shell. The true geometry and overall simplified geometry for the shell method is shown in Figure 20.

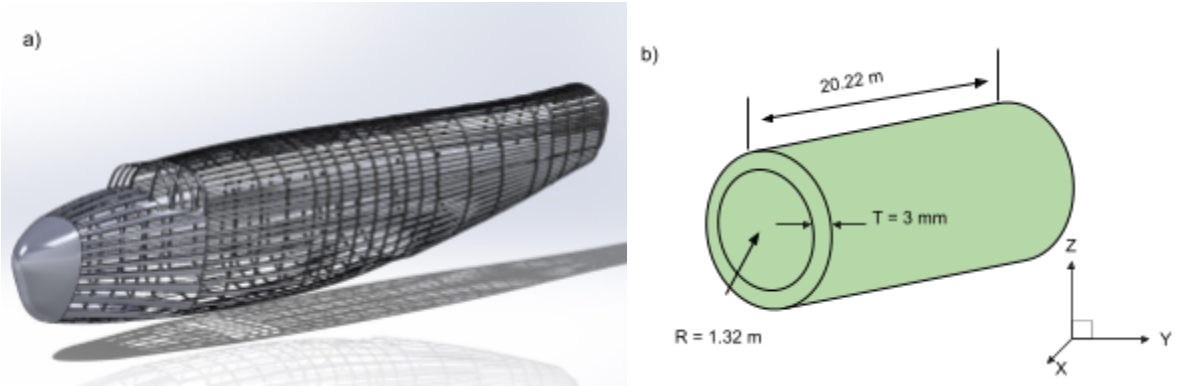


Figure 20: (a) B-24 Fuselage Structure (b) Simplified Model for Stiffened Shell Analysis

For the stiffened shell method, there were 33 frames and 50 longerons added, with their dimensions shown in Figure 21, where each frame and longeron shares the same cross sectional geometry.

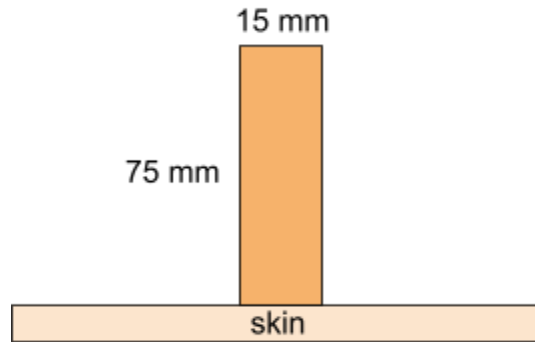


Figure 21: Frame and Longeron Geometry

The following sections detail the methodology, results, and validation of stiffened shell analysis.

8.1 Methodology

The methodology for stiffened shell analysis is followed similarly to shell analysis from Section 7.0, where the equations of motion are altered to Equations 46 to 48.

$$\frac{R(L_{R\theta})q_n}{E} = - \left(A_L - \frac{A_{SX}}{(v^2-1)} \right) [\xi] \quad (46)$$

$$\xi = \frac{v}{2} \left(\frac{\partial}{\partial \theta} \frac{\partial v}{\partial s} \right) + \frac{\partial^2 u}{\partial s^2} + \left(\frac{\partial}{\partial \theta} \frac{\partial v}{\partial s} + \frac{\partial^2 u}{\partial \theta^2} \right) (v - 1) \quad (46.a)$$

$$R^2 [q_b - m_\alpha] = \frac{-1}{L_{RX}} [\chi] - \frac{E}{L_{R\theta}} \left[v \left(\frac{A_{SX}}{(v^2-1)} \right) \left(\frac{\partial}{\partial \theta} \frac{\partial u}{\partial s} \right) - Y \right] \quad (47)$$

$$\chi = \left(\frac{\partial^2 v}{\partial \theta^2} + \frac{\partial w}{\partial \theta} \right) \left(A_f - \frac{A_{S\theta}}{(v^2-1)} \right) - \frac{E}{R} \left(I_{f\theta} - \frac{I_{SS}}{(v^2-1)} \right) \left(\frac{\partial^3 w}{\partial \theta^3} \right) \quad (47.a)$$

$$\begin{aligned} \Upsilon &= \left(\frac{v}{R^2} \right) \left(I_{LX} - I_{SX} (v^2 - 1) \left(\frac{\partial}{\partial \theta} \frac{\partial^2 w}{\partial s^2} \right) \right) \dots \\ &\quad \left(1 + \left(2 - \frac{2}{v} \right) \left(\frac{\partial}{\partial \theta} \frac{\partial u}{\partial s} \right) \right) - \left(\frac{\partial^2 v}{\partial s^2} + \frac{\partial}{\partial \theta} \frac{\partial u}{\partial s} \right) \left(\frac{A_{SX}}{2(v-1)} \right) \end{aligned} \quad (47.b)$$

$$\frac{R^2 q_n}{E} = \frac{1}{L_{R\theta}} (\Lambda) - \left(I_{LX} - I_{SX} (v^2 - 1) \right) \left(\frac{\partial^2}{\partial \theta^2} \frac{\partial^2 w}{\partial s^2} \right) \left[\frac{v}{R} - 8v - 8 \right] + \frac{1}{L_{RX}} [\Pi] \quad (48)$$

$$\Lambda = \left(I_{LX} - I_{SX} [v^2 - 1] \right) \frac{\partial^4 w}{\partial s^4} \left(\frac{1}{R} \right) + v \left[\frac{\partial u}{\partial s} \right] \left[A_L + \frac{A_{SX}}{(v^2-1)} \right] \quad (48.a)$$

$$\Pi = \left(A_f - \frac{A_{S\theta}}{(v^2-1)} \right) \left(\frac{\partial v}{\partial \theta} + w \right) + \left(I_{f\theta} - \frac{I_{SS}}{(v^2-1)} \right) \left(\frac{\partial^4 w}{\partial \theta^4} \right) \left(\frac{1}{R^2} \right) \quad (48.b)$$

where E is the young's modulus of 6061 aluminum, v is poisson's ratio, q_b is the applied load in the beta direction, and m_α is the applied moment in the alpha direction. Additionally, A_f and A_L represent the frame and longeron cross sectional areas respectively. A_{SX} is the cross sectional area of repeating axial sections, and $A_{S\theta}$ represents the cross sectional area of repeating angular sections. Respective L_{RX} , and $L_{S\theta}$ represent the length of repeating axial and angular sections. $I_{f\theta}$ is the area moment of inertia for frames about the circumferential direction, I_{SS} is the area moment of inertia for skin about the joint centroid between the frames and skin. I_{SX} and I_{LX} represent the area moments of inertia for skin and longerons about the joint centroid between the skin and longeron.

8.2 Results

For the intact case, the fuselage was found to first fail at a location 20.22 m along the fuselage, 136.5 degrees from the top centerline of the fuselage on the port side at a loading factor of 6.42. The second failure occurs at a location 0 m along the fuselage at the same circumferential location and at a loading factor of 6.85. The stress in the fuselage is shown in Figure 22.

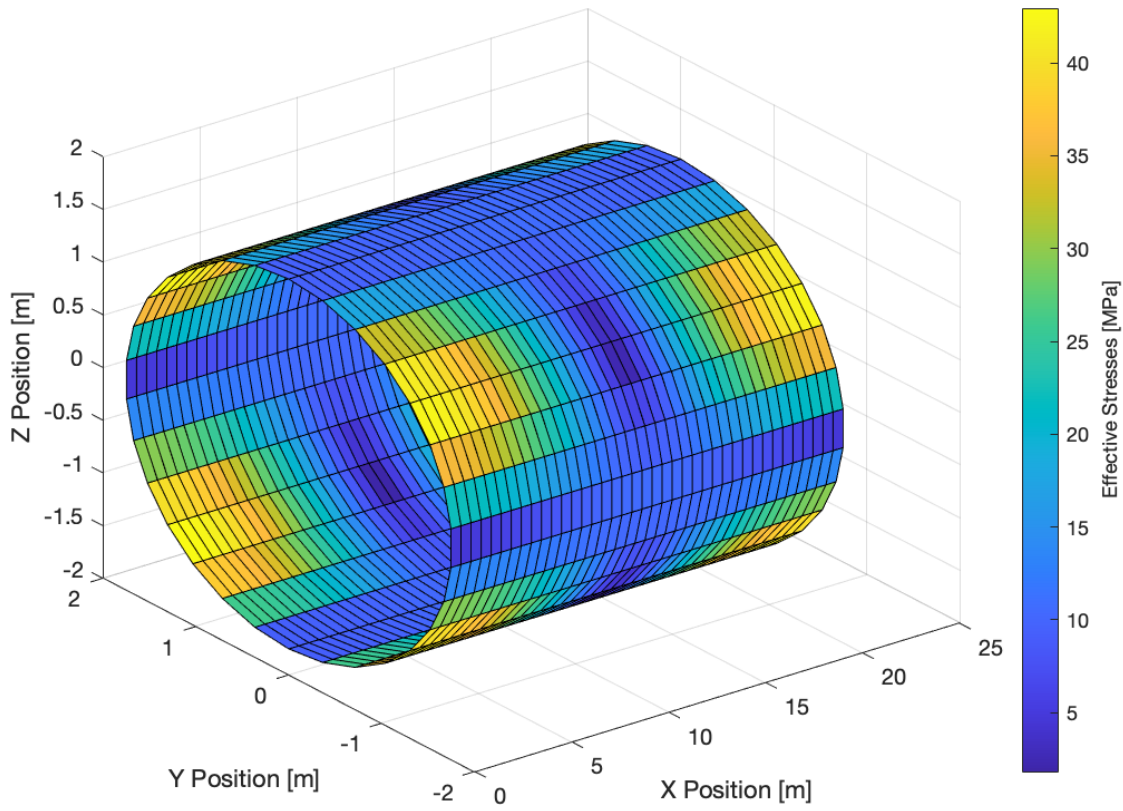


Figure 22: Effective Stress in the B-24 Fuselage As Predicted By Stiffened Shell Analysis

8.3 MATLAB Validation

Validation of the stiffened shell analysis was performed by comparing it against experimental data [21]. The validation case applied axial compression to a stiffened shell and measured results via strain gauges. Circularity of the test specimens was preserved through wooden or aluminum bulkheads. An error of 31.68 % was realized.

9.0 Conclusion

The analyses conducted on the Consolidated B-24 fuselage include applied loads, beam bending, multi-cell web-stringer, circular and rectangular plates, and simple and stiffened shell analysis. The load factors and locations of failures in the fuselage are shown in Figure 23.

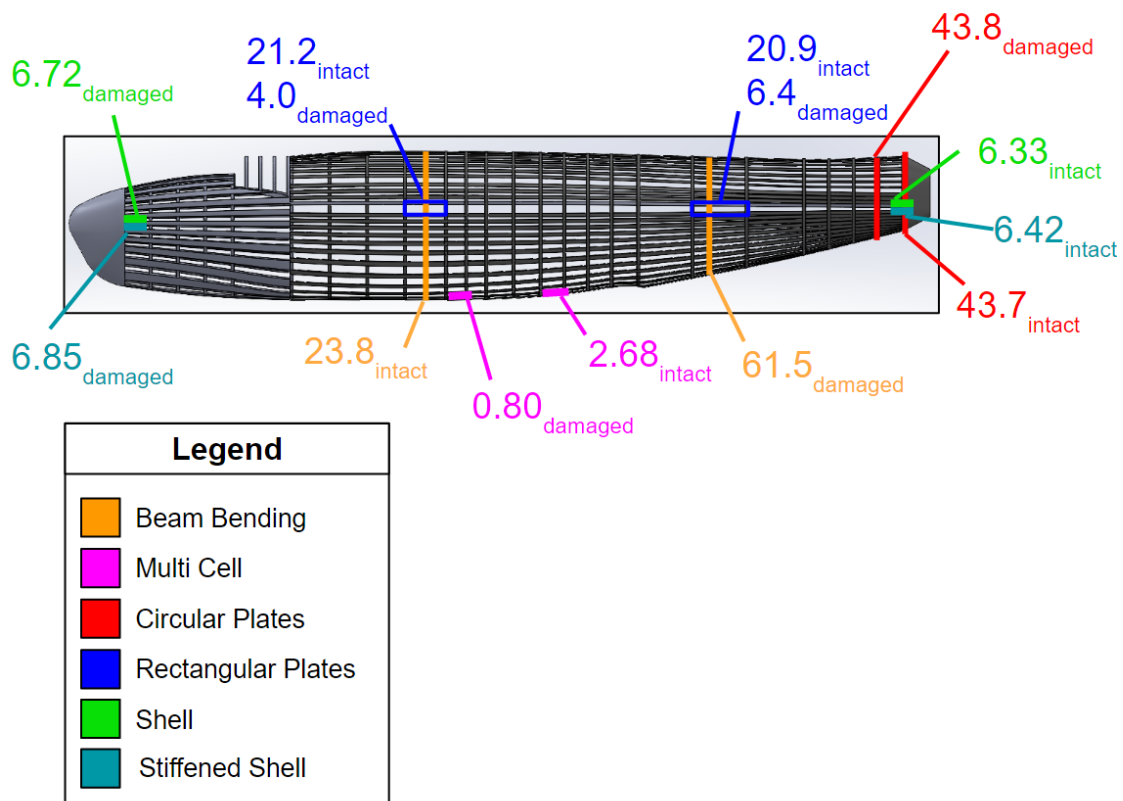


Figure 23: Failure Locations and Load Factors for Each Analysis

The group places the most trust in the multi-cell web-longeron analysis because the load factors are most in line with the expected magnitude, and this analysis is capable of analyzing individual longerons and skin panels as a cohesive system. The stiffened shell method is also capable of analyzing a cohesive system. The locations of failure for stiffened shell analysis reduce the group's trust in this method, because no loads are applied at the locations of failure to cause stress.

References

- [i] S. Slocum, *B-24 DIAMOND LIL*. 2023.
- [1] “The B-24: The great liberator,” Lockheed Martin, 12-Aug-2022. [Online]. Available: <https://www.lockheedmartin.com/en-us/news/features/history/b-24.html>. [Accessed: 18-Jan-2023].
- [2] “B-24,” *Encyclopædia Britannica*. [Online]. Available: <https://www.britannica.com/technology/B-24>. [Accessed: 18-Jan-2023].
- [3] “42-40506,” American Air Museum. [Online]. Available: <https://www.americanairmuseum.com/archive/aircraft/42-40506>. [Accessed: 06-Mar-2023].
- [4] S. D. A. S. M. Archives, “Lindell Hendrix Special Collection,” *Flickr*, 2023. [Online]. Available: <https://www.flickr.com/photos/sdasarchives/sets/72157633769465617>. [Accessed: 17-Jan-2023].
- [5] “Hendrix (Lindell Eugene) personal papers,” *Online Archive of California*. [Online]. Available: <https://oac.cdlib.org/findaid/ark:/13030/c890270z/?query=Hendrix%2B%28Lindell%2BEugene%29%2BPersonal%2BPapers>. [Accessed: 17-Jan-2023].
- [6] “Lindell Hendrix,” *Lindell Hendrix - WWII Serviceman - 491BG - 0*, 2023. [Online]. Available: <https://www.8af.org/hendrix-lindell-h7800-491bg.cfm>. [Accessed: 17-Jan-2023].
- [7] “491st Bomb Group | American Air Museum,” *491st Bomb Group*, 07-Jul-2019. [Online]. Available: <https://www.americanairmuseum.com/archive/unit/491st-bomb-group>. [Accessed: 17-Jan-2023].
- [8] J. Rickard, *491st Bombardment Group*, 06-Feb-2008. [Online]. Available: http://www.historyofwar.org/air/units/USAAF/491st_Bombardment_Group.html. [Accessed: 17-Jan-2023].

- [9] R. Darling, “Consolidated B-24 Liberator , Hobbymaster new models due mid-March, and Herpa announcements.,” *Flying Tigers*, 19-Feb-2021. [Online]. Available: <https://www.flying-tigers.co.uk/2021/consolidated-b-24-liberator-hobbymaster-new-models-due-mid-march-and-herpa-announcements/>. [Accessed: 17-Jan-2023].
- [10] “San Diego Air & Space Museum - Balboa Park, San Diego,” *Lindell Eugene Hendrix Personal Papers*. [Online]. Available: <https://sandiegoairandspace.org/collection/item/lindell-eugene-hendrix-personal-collection>. [Accessed: 17-Jan-2023].
- [11] W. H. Plunkett, in *F-105 Thunderchiefs: A 29-year illustrated operational history, with individual account of the 103 surviving fighter bombers*, Jefferson, NC: Mcfarland, 2008, pp. 27–32.
- [12] L. Hendrix, “Aerospace Safety.” Feb-1963.
- [13] “Consolidated B-24 Liberator,” Classic Warbirds - Bringing Vintage Aircraft to Life. [Online]. Available: <https://www.classicwarbirds.co.uk/american-aircraft/consolidated-b-24-liberator.php>. [Accessed: 07-Mar-2023].
- [14] “Consolidated B-24 Liberator 3D model,” Consolidated B-24 Liberator 3D Model - 3D CAD Browser. [Online]. Available: <https://www.3dcadbrowser.com/3d-model/consolidated-b-24-liberator>. [Accessed: 11-Feb-2023].
- [15] T. Trainor, “How Ford's Willow Run Assembly Plant helped win World War II,” *ASSEMBLY RSS*, 03-Jan-2019. [Online]. Available: <https://www.assemblymag.com/articles/94614-how-fords-willow-run-assembly-plant-helped-win-world-war-ii>. [Accessed: 23-Feb-2023].
- [16] “MatWeb - The Online Materials Information Resource,” www.matweb.com.
<https://www.matweb.com/search/DataSheet.aspx?MatGUID=b8d536e0b9b54bd7b69e4124d8f1d20a>

- [17] M. D. Bashir, “Experiment No. 2: Deflection of a Cantilever Beam.” 2018.
- [18] F. A. Johnsen, *Consolidated B-24 Liberator*. North Branch, MN: Specialty Press, 1996
- [19] L. Kovalevsky, T. Furuike, L. A. Nelson, and F. L. Rish, “Analysis of Webs of Partial-Tension-Field Beams Subjected To Lateral Pressure Loadings.” Apr-1966.
- [20] W. J. Leumont, “Collapse Tests of Pressurized Membrane-Like Circular Cylinders for Combined Compression and Bending.” May-1965.
- [21] J. P. Peterson and M. B. Dow, “Compression Tests on Circular Cylinders Stiffened Longitudinally by Closely Spaced Z-Section Stringers.” Mar-1959.

Appendix

Attached in the following appendices are Engineering Drawings, and MATLAB code used for calculations.

Computer Assisted Design (CAD) Dimensioned Assembly:

